2014년 12월 전자공학회 논문지 제 51권 제 12 호
Journal of The Institute of Electronics and Information Engineers Vol. 51, NO. 12, December 2014 http://dx.doi.org/10.5573/ieie.2014.51.12.111

논문 2014-51-12-12

시각 부호화 마커를 이용한 환자의 호흡 추적

(Patient Respiratory Motion Tracking Using Visual Coded Markers)

우다야 위제나야키*, 박 순 용**

(Udaya Wijenayake and Soon-Yong Park©)

요 약

방사선요법이 암의 치료에 널리 사용되는 방법 중의 하나가 되면서 호흡에 의한 환자 움직임의 정확한 추적은 치료 계획이나 조사량 계산에 있어 매우 중요한 요소가 되고 있다. 호흡에 의한 움직임의 부정확한 추적은 일반 조직의 오류나 높은 준위의 방사선에 노출되는 건강한 조직의 범위를 확대시키는 심각한 논란을 야기할 수 있다. 다양한 호흡 예측에 대한 기술이 연구가 되었지만, 대부분의 기술들은 특정 전자장치나 고가의 부품을 필요로 하였다. 본 논문에서는 기존의 기술에 비하여 저가이고 사용이 간편한 대안으로서 스테레오 비전 기술을 이용하여 시각 코드 타겟을 추출하고 복호화하여 새로운 3차원 호흡 추적 방법을 제안한다.

Abstract

As radiotherapy has become one of the widely used techniques in cancer treatment, accurate tracking of patient's respiratory motion is considered to be more important in treatment planning and dose calculations. Inaccurate motion tracking can cause severe issues such as errors in target/normal tissue delineation and increasing the volume of healthy tissues exposed to high doses. Different methods have been introduced to estimate the respiratory motion, but most of them require some electronic devices or expensive materials. As an inexpensive and easy to use alternative to the previous methods, we propose a new 3D respiratory motion tracking method by using stereo vision techniques of detecting and decoding visual coded markers.

Keywords : Respiratory motion, visual coded markers, stereo vision

Ⅰ. Introduction

Radiotherapy is a widely used technique, generally as a part of cancer treatment to control or kill malignant cells. In the era of image-guided radiotherapy, respiratory motion tracking has attracted a lot of research attentions as it induces significant internal movements while causing many problems like image acquisition limitations, treatment planning limitations and radiation delivery limitations[1].

1.1 Respiratory Motion

If the respiratory motion is not accounted correctly, motion artifacts can be resulted in CT images and affected to target/normal tissue delineation and dose calculation accuracy. In treatment planning, adding margins to cover the limits of the motion may

* 학생회원, ** 평생회원, 경북대학교 컴퓨터학부
(School of Computer Science and Engineering, Kyungpook National University)
© Corresponding Author(E-mail: sypark@knu.ac.kr)
※ 본 연구는 미래창조과학부 및 정보통신기술진흥센터의 정보통신·방송 연구개발사업[10043897, 치료시간 30% 단축을 위한 자동 병변 추적 기술기반 악성종양 치료용 500cGy급 dual-head 갠트리 방사선 치료시스템 개발] 및 2014년도 경북대학교 학술연구비의 일환으로 수행되었음.
접수일자: 2014년06월18일, 수정일자: 2014년10월20일
게재확정: 2014년11월25일

increase the radiation field size and consequently the volume of healthy tissues exposed to high doses. On the other hand, if the margins are not large enough, part of the clinical target volume will not receive advocate dose coverage. In the phase of radiation delivery, presence of respiratory motion causes an averaging or blurring of the static dose distribution over the path of the motion.

As a solution to these problems, many different methods, such as motion encompassing, respiratory gating, breath holding, forced shallow breathing with abdominal compression, and real-time tracking, have been introduced to handle the respiratory motion. Before delivering treatments, motion encompassing techniques require a series of scans on the affected area to be taken over several complete respiratory cycles to understand the movements of the tumor. Then a 3D volume (space) which represents the positions of the tumor during the whole respiratory cycle is created. This whole volume is used as the treatment delivery area and consequently some healthy tissues might get exposed to high doses. In breath-holding techniques, patient is asked to hold the respiration for short intervals and deliver treatments during these intervals. However, this technique is especially difficult for patients having a compromised pulmonary function which is the case for most of the lung cancer patients. Forced shallow breathing techniques use a physical plate over the abdominal region to restrict the breathing motion which causes more inconveniences for the patient. Respiratory gating techniques use an external marker to calculate the respiratory cycle and periodically turn on the treatment beam when the breathing parameters fall within a predefined range[2]. These breath-holding and gating techniques have extra burden such as handling patient movements, longer treatment time, patient training and model instability.

Real-time target tracking techniques have been proposed to solve these problems by actively estimating the motion and continuously synchronizing beam delivery with the motion of the tumor. The Calypso, prostate motion tracking system integrated in Varian (Varian Medical Systems, Palo Alto, CA), implants three tiny transponders shown in Figure 1(c) into the prostate to send tracking signals to the system[3]. When the prostate moves outside the planned treatment area, the radiation beam can be stopped to minimize the damage to the healthy tissues. The BrainLAB ExacTrac positioning system uses implanted fiducial markers with external infrared reflecting markers (Figure 1(b)) to align the patient and gates the treatment beam[4]. The Synchrony respiratory tracking system, a subsystem of CyberKnife, is the first technology which continuously synchronize beam delivery to the motion of the tumor[5]. The motion is tracked using a fiber optics marker vest shown in Figure 1(a).

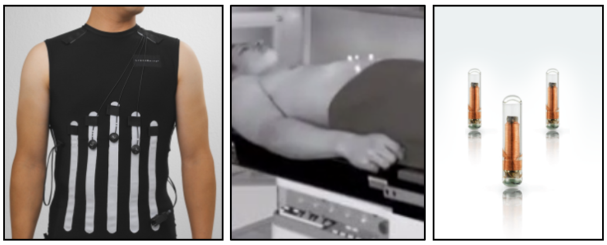

(a) (b) (c)

그림 1. 방사선 요법에 사용되는 다양한 종류의 호흡 추적 시스템

Fig. 1. Various types of motion tracking systems used in radiotherapy.

1.2 Proposed Method

Most of the previous real-time respiratory motion tracking techniques use electronically connected devices or expensive materials as markers. Instead of using such inconvenient and complicated markers, we propose a respiratory motion tracking technique using visual coded markers (AR markers) which are cost effective and easy to handle.

First, an introduction to visual coded markers is given in Section Ⅰ.3 with an overview of the proposed system in Section Ⅱ. In Section Ⅲ, the properties of the proposed marker system are

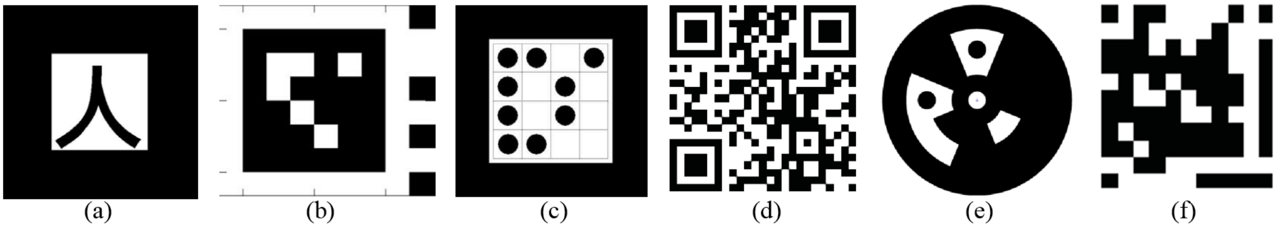

그림 2. 여러 종류의 시각 부호화 마커 (a) ARToolKit 마커[6] (b) Hoffman 마커[7] (c) 지멘스 연구소 마커[8] (d) QR 코드 (e) Intersense 마커[9] (f) Rohs 마커[10]

Fig. 2. Different types of visual coded markers (a) ARToolKit markers[6] (b) Hoffman marker[7] (c) Siemens Corporate Research (SCR) marker[8] (d) QR Codes (e) Intersense marker[9] (f) Rohs's visual codes[10].

explained along with the encoding algorithm. The image processing algorithms – which are used to automatically locate the markers on a stereo image pair – are explained in Section Ⅳ. The way of extracting embedded code information from the detected markers using the projective transformation matrix is explained in section Ⅳ.3. The procedure of calculating 3-dimensional information (using previously obtained code information) and the motion parameters of each marker is discussed in section Ⅴ. Finally, the experiments conducted to analyze the accuracy of the proposed system are explained in Section Ⅵ.

1.3 Visual Coded Markers

Visual coded markers are mostly 2-dimensional binary images embedded with code information which can be used later to uniquely identify the markers. They are mostly used in augmented reality (AR) applications for tracking and pose estimation purposes. Examples of some visual coded markers used in existing AR applications are shown in Figure 2[6~10].

The performance of such an AR system highly depends on marker detection, decoding and pose estimation accuracy[11] where the performance requirements differ based on the application. In the case of proposed method, a higher performance level is required as it is going to be implemented in respiratory motion tracking system for radiotherapy.

Among those different kinds of markers, square-shaped markers are the most commonly used ones because their four corner information can be used to estimate the pose of the markers without using any neighboring marker information. Camera calibration also can be done using the four corner information of a single marker. Circular (co-centric) markers, mostly used in previous respiratory motion tracking systems, can only provide one point-correspondence per a marker and at least three markers in the same image are required to estimate the pose.

Ⅱ. System Overview

Visual coded markers are designed in smaller sizes as possible, in order to attach them to the affected area of the human body. A calibrated stereo camera is used to capture two different views of the attached marker and different image processing algorithms are used to track the marker in real-time. The 3D coordinates of each marker corners can be calculated using the relevant 2D coordinates of the marker corners in left and right images. Then these 3D

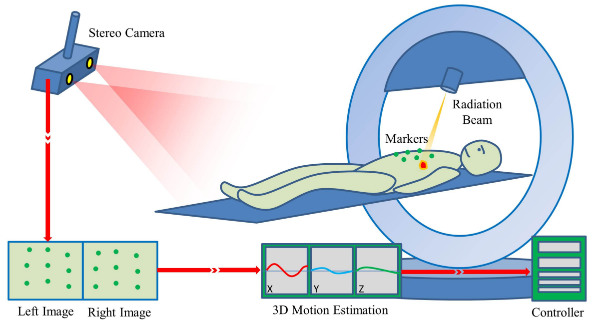

그림 3. 제안한 마커 추적 시스템의 적용 예

Fig. 3. Application example of the proposed marker tracking system.

coordinates are used to estimate the motion of the attached surface. Figure 3 shows an overview of the proposed system.

Ⅲ. Marker Encoding

The visual coded markers we use in our proposed system are based on ARTag[12], a marker system which uses digital coding theory to get a very low false positive and inter-marker confusion rate with a small marker size (very important when being used on a human body). The ARTag marker system contains 2002 planar markers, where each marker consists of a black or white square border and an interior region filled with a 6×6 grid of black or white cells. In the proposed marker system, only a black square border with a reduced interior grid of 3×3 is used, as a few number of markers are needed to cover a specific area of a human body. The marker can hold a 9bit binary code-word where each bit corresponds to its respective cell value in the grid. Each cell value in the grid can be either '1' or '0' according to the color (white or black respectively) it holds.

When encoding the 3×3 grid with a binary code-word, a random assigning process with three constraints is used. The first constraint is that at least one cell which is connected to the black border should be filled with black color. This restriction is imposed to avoid two near square contours which could cause difficulties in marker detection process. According to the second constraint, when the filled grid is rotated in four different angles $(0^0, 90^0, 180^0, 270^0)$; the four output code-words should be different from each other. Then the output code-word of the grid with 0^0 rotation is taken as the representative code-word of the marker. If a code-word similar to previous ones or their three rotations is found in the proceeding iterations, that code-word is rejected to keep the uniqueness of the markers, which is the third constraint of the marker

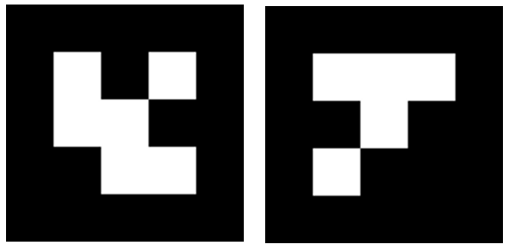

[101 110 011] [111 010 100]

그림 4. 제안 시스템에 사용된 두 마커의 예와 그 부호단어

Fig. 4. Two example markers and its code-words used in proposed system.

encoding process. 120 different markers are generated adhering to all of the above constraints and two of them are shown in Figure 4.

Ⅳ. Marker Detection and Decoding

Proposed marker tracking algorithm consists of three main modules: 1) Pre-processing of the camera images; 2) Coded marker detection from the processed images; and 3) Extraction of embedded code data from the detected markers. Figure 5(a) shows a typical input image which will be used for illustrating the algorithm.

4.1 Image Pre-Processing

The objective of this step is to produce a binary image from the input camera image, which has an accurate representation of each visual coded marker in the image. When converted to a binary image, an image pixel can be represented by 1 bit instead of 24 bits used in color images . This reduction of data will help to decrease the computational time without losing any relevant data from the markers as they contain binary code-words only. Further, binarization will help to design a simple and computationally efficient algorithm to detect markers from input images.

In the proposed system, an adaptive thresholding technique[16] is adopted to convert a grayscale image to a binary image that compensates the uneven

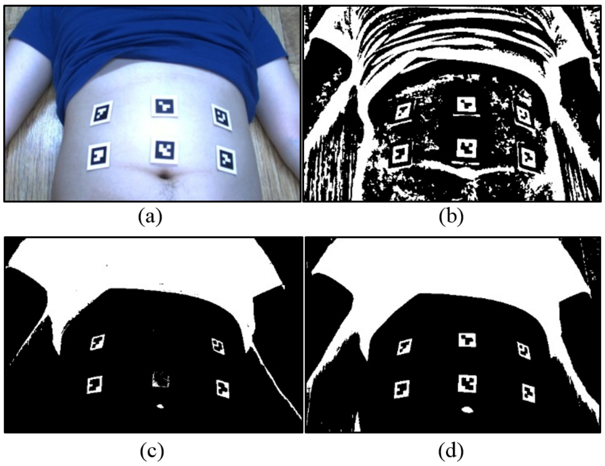

그림 5. 영상의 임계값 적용 결과 (a) 입력영상 (b) 적응적 지역 임계값 (c) 전역 임계값=60 (d) 전역 임계값=100

Fig. 5. Image thresholding results (a) Input image (b) Adaptive local thresholding (c) Global threshold=60 (d) Global threshold=100.

camera brightness, varying scene illumination, and image noise. In contrast to global thresholding, adaptive thresholding is a local thresholding technique that computes separate threshold values for each pixel based on the neighborhood. Intensity value of each pixel is compared with the weighted sum of its neighbors with a Gaussian kernel to decide whether it is black or white as shown in Equation (1), where $T(x,y)$ is the weighted sum and c is a user defined constant. The user has to select the window size and the constant c according to the image size, marker size, and the average brightness level of the images.

$$dst(x,y) = \begin{cases} 0 & \text{if } src(x,y) > T(x,y) - c \\ 255 & otherwise \end{cases} \tag{1}$$

In the proposed system, an inverse thresholding technique is used to simplify the detection step. Figure 5 shows a comparison between the adaptive thresholding technique and the global thresholding with different threshold values.

4.2 Marker Detection

Identification of the coded markers in the binary images relies on their common feature: black square border. To clearly differentiate the black border from the image scene, especially from darker backgrounds, another small white border is added around the black border.

As the first step of the marker decoding process, a contour detection algorithm is applied on the binary image to label the connected regions. Then the contour size is used to eliminate too large or small regions which are possibly not markers. Three properties of the square-shaped visual coded markers; having four sides, being a parallelepiped and convex, are used to filter out the regions which are not corresponding to markers. In order to do that, each remaining contour is approximated to a polygon using the Douglas-Peucker algorithm[17] and analyze the shape. If the approximated polygon is not convex or does not have exactly four sides, these contours are disregarded as possible markers. Furthermore, the length of the four sides of the polygon is analyzed to remove the contours which are not parallelepiped.

Figure 6 (a) and (b) show the results of contour

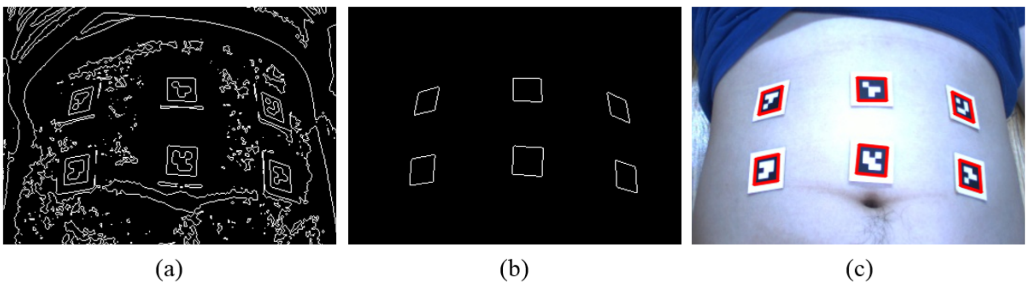

그림 6. 마커 검출 및 복호화 과정 (a) 외곽선 추출 (b) 정제된 외곽선 (c) 복호화 예정인 마커 영역의 추출

Fig. 6. Process of marker detection and decoding (a) Contour detection (b) Refined contours (c) Detected possible markers which will send to decoding stage.

detection and contours refinement respectively. After completing all the refinements, remaining contours are considered as possible markers. Then the four corners of each marker are refined by applying a sub-pixel level corner finding method to increase the accuracy of the detected marker position. Figure 6(c) shows the refined detected possible markers.

4.3 Marker Decoding

The main goal of the marker decoding process is to extract the embedded code data from the detected markers. In this process, first the projective transformation between the image plane and the code plane is computed accurately using the four corner information of each marker in both plane. The sub-pixel level coordinates of the four corners in the image plane can be found from the marker detection process whereas the coordinates in code plane are already known by the definition of the marker size. Then each detected marker (Figure 7(a)) is transformed to the code plane (Figure 7(b)) and apply binary thresholding in order to clearly identify the data area. Otsu's method[15]; a less time consuming adaptive thresholding technique which defines a global threshold value analyzing an image histogram; is applied here since it works well on small images like Figure 7(b) which do not contain much variations.

As shown in Figure 7(c) a 5×5 mask is applied on that binary image and proceed through the known data areas according to the definition of the markers and test for the logical state by analyzing the pixel values. In this way, the 9 bits binary code-word embedded in the 3×3 inside grid of the marker can be obtained. Then a look-up table is used to identify the marker ID from the binary code-word. If the code-word cannot be found directly in the look-up table, it is rotated either to 90^0, 180^0 or 270^0 and searched through the lookup table again. By following this process, both the ID and orientation of the maker can be found at once. This decoding process is illustrated in Figure 7, and it is applied to both left and right camera images to get marker information in both views.

그림 8. 다양환 상황에서의 마커의 검출 및 복호화 결과

Fig. 8. Marker detection and decoding results in different situations.

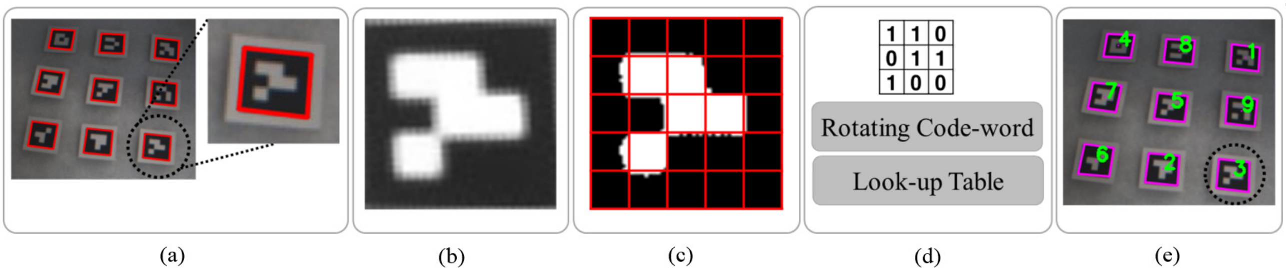

그림 7. 시각 마커의 복호화 과정 (a,b) 마커 추출 영역과 투영변환 결과 (c) 마커의 이진코드 생성을 위한 5x5 마스크 설정 (d) 코드워드의 회전과 LUT를 이용한 마커 ID 결정 (e) 마커 인식 결과

Fig. 7. Visual coded marker decoding process. (a) & (b) Applying projective transformation to each detected markers to get the orthogonal view (code plane). (c) Applying 5×5 window mask to get the binary code-word. (d) Use rotation and look-up tables to get the code ID. (e) Marker recognition results.

In different lighting and environmental conditions, the proposed marker detection and decoding method works well without false positive or inter-marker confusions. Some results of the marker detection and decoding are shown in Figure 8. These results prove that the proposed method is invariant to background condition and also robust to various illumination levels and different marker angles.

V. Motion tracking

After finding the marker IDs and their coordinate information on both views, camera calibration parameters with triangulation[13] techniques can be used to find the 3D coordinates of each marker as shown in Figure 9.

Using this 3D information, displacement, acceleration, and rotation information of each marker can be calculated independently. Displacement of a marker M at time t can be defined by Equation 2, where $m_t(x,y,z)$ represents the 3D location of the marker. Acceleration A of a marker M at a given time t can be calculated by Equation 3 using the displacement information. If the centroid (c_t) of the marker is found using four corner information m_t^i, rotation R can be found using SVD as shown in Equation 4 and 5.

$$D_t(M) = m_t(x,y,z) - m_{t0}(x,y,z) \tag{2}$$

$$A_t(M) = [D_{t-2}(M) - 2D_{t-1}(M) + D_t(M)]/\Delta t^2 \tag{3}$$

$$H = \sum_{i=1}^{4} (m_t^i - c_t)(m_{t0}^i - c_{t0}) \tag{4}$$

$$[U,S,V] = SVD(H),\ \ R_t(M) = VU^T \tag{5}$$

Ⅵ. Experiments

6.1 Experiment Setup

The proposed method is implemented in a vision system which is composed with two Point Grey FL3-FW-20S4C-C CCD cameras; each having a 6mm lens and capable of providing stereo images of 800×600 resolution. The baseline between the two cameras is about 10cm and the focus of the camera is set to be around 70cm from the camera. All the computations are done in a common PC with a 2.67 GHz Core i5 CPU and 4GB RAM. OpenCV library is used for image processing tasks and OpenGL is used for some visualization parts. The Zhang's[14] camera calibration method is used to calibrate the stereo camera.

6.2 Respiratory Motion Analysis

An experiment is conducted to analyze the human respiratory motion by attaching six markers to the

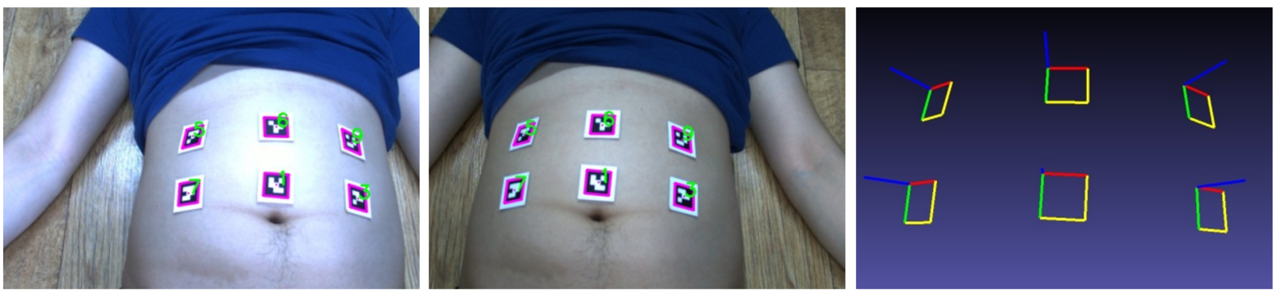

(a) (b) (c)

그림 9. 스테레오 영상의 마커 검출 및 3차원 정보 계산 (a) 좌영상 (b) 우영상 (c) 마커의 3차원 자세
Fig. 9. Marker detection results of a stereo view and the calculated 3D information.
(a) Left image (b) Right image (c) 3D pose of markers.

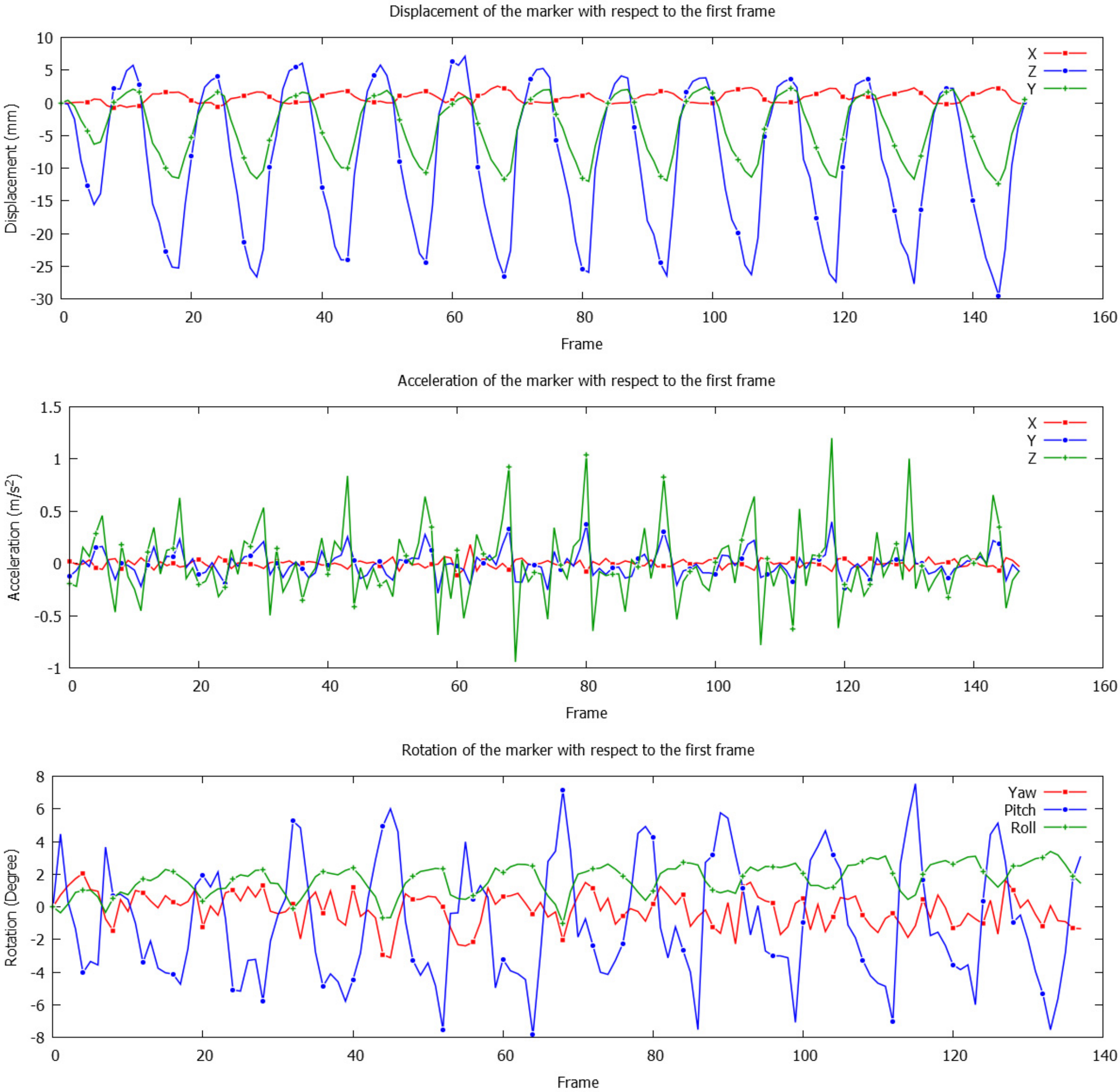

그림 10. 환자 복부에 장착된 마커의 움직임 분석 기준프레임에 대한 마커의 (a) x,y,z 축 변위 (b) x,y,z 축 가속도 (c) Yaw, Pitch 및 Roll 회전

Fig. 10. Motion analysis of a selected marker attached to the human abdomen (a) Displacement and (b) Acceleration of the marker in x, y and z axises (c) Rotation of the marker in Yaw, Pitch and Roll with respect to the reference frame.

abdomen as shown in Figure 9(a). Then the markers are tracked continuously for about one minute, starting from an end-exhale position. Using the equations given in Section 5 and selecting the first frame as the reference frame, the displacement, acceleration, and rotation of each markers are estimated for every frame. In the case of acceleration, estimation is started from the third frame as the displacement information of two previous frames is required to calculate the acceleration. Three graphs in Figure 10 depict the estimated displacement, acceleration and rotation information of a selected marker for 150 consecutive frames in x, y, and z axises.

6.3 Accuracy Analysis

Using the experiment explained in Section 6.2, the accuracy of the motion tracking cannot be analyzed as the ground truth of the human respiratory motion is not available. Therefore, another experiment is conducted to analyze the accuracy of our proposed system by tracking a motion with a known ground truth. In this experiment, the coded marker is moved for an accurately measured distance along a linear motion stage and that distance is measured using the proposed method. Figure 11 shows the experimental setup which consists of the stereo camera, linear motion stage, coded marker and the controllers for the stereo camera and motion stage.

As shown in the Figure 12, the marker is moved 300mm vertically along the linear motion stage and tracked its motion in different angles and distances by changing the position of the stereo camera. The markers are placed in different orientations (in angle and distance) with reference to the camera when they are attached to a human body. In the experiment setup, the stereo camera is placed in five different angles (-45°, -30°, 0°, +30°, +45°) and three different distances (60 cm, 70 cm, 80 cm) to simulate this situation instead of using multiple markers. Table 1 gives the results of the experiment where the first column represents the angle of the stereo camera to

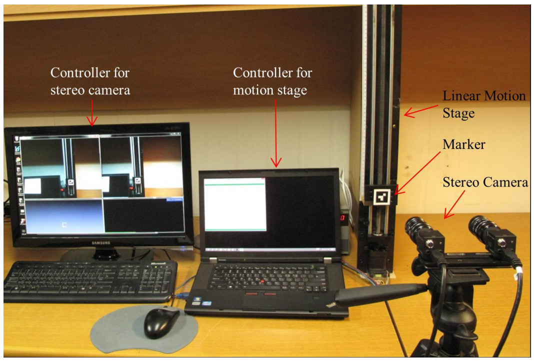

그림 11. 스테레오 카메라와 선형 스테이지 기반의 실험 장치

Fig. 11. Experiment setup with the stereo camera and the linear motion stage.

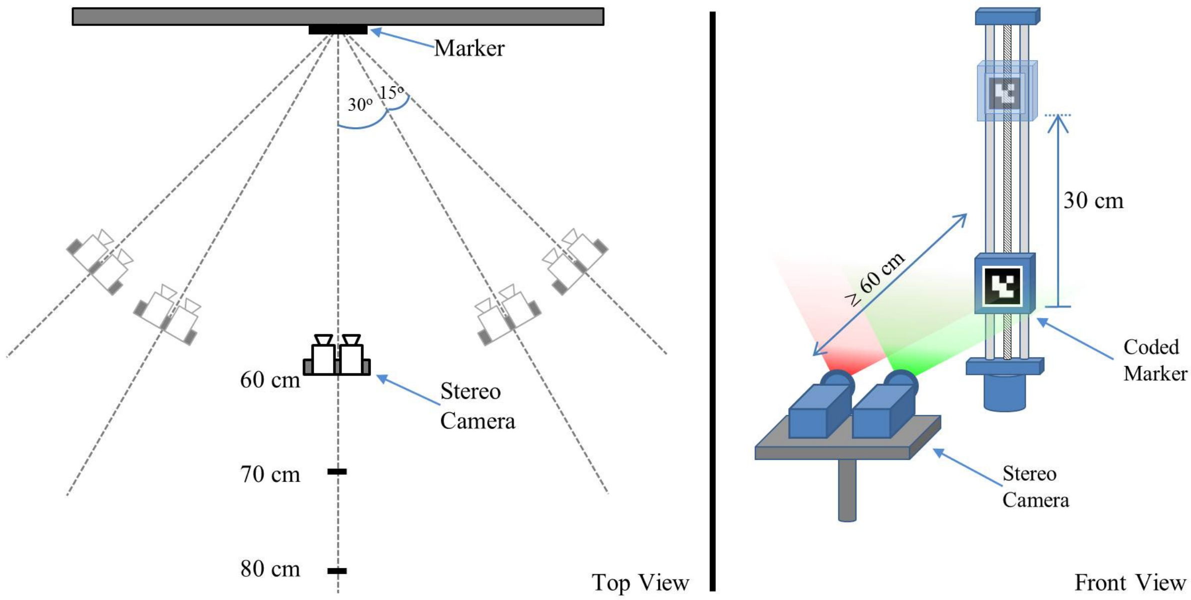

그림 12. 제안 시스템의 정밀도 분석을 위한 실험 장치. 좌측은 다양한 실험 데이터 획득을 위하여 스테레오 카메라의 설치 위치를 변경함을 보여줌. 우측은 스테레오 카메라 위치 및 마커의 이동 경로를 보여줌.

Fig. 12. Experiment setup for analyzing the accuracy of the proposed system. Left image shows the top view of the experiment setup which explains how the position of the stereo camera changed. Right image shows the front view which explains how the marker is moved.

표 1. 참값(ground truth)과의 비교를 통한 제안한 호흡 추적 시스템의 정밀도 측정 결과
Table 1. Measuring the accuracy of the proposed motion tracking technique by comparing it with the ground truth.

Angle	(cm)	(mm)	Error (%)
-45°	60	300.40	0.13
	70	300.35	0.12
	80	301.08	0.36
-30°	60	300.75	0.25
	70	300.52	0.17
	80	301.32	0.44
0°	60	300.84	0.28
	70	300.25	0.08
	80	300.91	0.30
+30°	60	300.32	0.11
	70	299.96	0.01
	80	300.35	0.12
+45°	60	299.36	0.21
	70	300.05	0.02
	80	300.72	0.24
Average	70	300.48	0.19

the orthogonal view of the maker, the second column represents the horizontal distance from the camera to the marker, the third column represents the displacement of the marker measured by the proposed method, and the last column represents the percentage of the measurement error compared to the ground truth (300mm).

As shown in the Table 1, the average measured displacement is 300.48mm and the average error percentage is ±0.19. Due to the focus setting of the camera, the most accurate results in all cases are obtained when the distance between the camera and the marker is 70cm. When the marker is too close or far from the camera, captured images will be out of focus and cannot detect the marker corners accurately.

6.3 Accuracy Comparison

Conducting an experimental level accuracy comparison within a laboratory environment is not feasible as most of the related work mentioned in Section Ⅰ.1 are highly expensive commercial products. Therefore, accuracy of the proposed system is compared with three previous systems which have related publications with accuracy analysis. Most of the respiratory motion tracking systems consider three different motions; anterior/posterior (AP), superior/inferior (SI), and lateral/medial (LM) during the accuracy analysis. During the accuracy analysis of the proposed method, SI motion is simulated by the movement of the marker where as AP and LM motion is simulated by changing the position of the stereo camera. Table 2 gives the accuracy comparison results which proves that the proposed method is quite compatible with the other three systems.

표 2. 기존의 세 종류의 호흡 추적 시스템과 제안 방법의 측정 정밀도 비교
Table 2. Accuracy comparison of the proposed method with three related respiratory motion tracking systems.

System	Accuracy
Synchrony[5]	< 1.5 mm
ExacTrac[4][18]	< 1.0 mm
Calypso[3]	< 1.5 mm
Proposed Method	< 1.3 mm

Ⅶ. Conclusions

In this paper, we proposed a respiratory motion tracking system using visual coded marker tracking technique with a stereo camera. Currently the tracking process takes an average of 0.25 seconds to process a pair of left and right camera images as the image resolution is high.

The accuracy of an AR marker detection method basically based on three criterion; false negative, false positive, and inter-marker confusion. False positive is the case that a marker is detected even it does not exist in real, whereas false negative is defined to be the opposite of false positive. The inter-marker confusion is the case that a marker is detected, but the wrong id was given, i.e. one marker was mistaken for another.

Using our experiment we figured out that, when a visual coded marker is detected correctly, the embedded code-word of the maker can be read out accurately without inter-marker confusion. While performing the experiments, the proposed method did not show any false positives but few false negatives. We figured-out that the inconsistencies in the detection process was the reason which caused false negatives.

More experiments were conducted to analyze the accuracy of the motion tracking by comparing it with ground truth and the results prove that the proposed system can achieve an acceptable accuracy level. In order to enhance the robustness of the marker detection process, we are planning to introduce some image enhancing techniques to improve the captured images. We are also working on reducing the processing time by enhancing the efficiency of the algorithm.

REFERENCES

[1] P.J. Keall, G.S. Mageras, J.M. Balter, R.S. Emery, K.M. Forster, S.B. Jiang, et al, The management of respiratory motion in radiation oncology report of AAPM Task Group 76, Med.Phys. 33 (2006) 3874-3900.

[2] C. Saw, E. Brandner, R. Selvaraj, H. Chen, M.S. Huq, D. Heron, A review on the clinical implementation of respiratory-gated radiation therapy, Biomed. Imaging Intervention J. 3 (1) (2007) e40.

[3] T.R. Willoughby, P.A. Kupelian, J. Pouliot, K. Shinohara, M. Aubin, M. Roach III, et al, Target localization and real-time tracking using the Calypso 4D localization system in patients with localized prostate cancer, Int. J. Radiat. Oncol. Biol. Phys. 65 (2) (2006) 528-534.

[4] J. Jin, F. Yin, S.E. Tenn, P.M. Medin, T.D. Solberg, Use of the BrainLAB ExacTrac X-Ray 6D system in image-guided radiotherapy, Med. Dosim. 33 (2) (2008) 124-134.

[5] Y. Seppenwoolde, R.I. Berbeco, S. Nishioka, H. Shirato, B. Heijmen, Accuracy of tumor motion compensation algorithm from a robotic respiratory tracking system: a simulation study, Med.Phys. 34 (2007) 2774- 2784.

[6] ARToolKit, http://www.hitl.washington.edu/artoolkit/.

[7] M. Appel, N. Navab, Registration of technical drawings and calibrated images for industrial augmented reality, Mach. Vis. Appl. 13 (3) (2002) 111-118.

[8] X. Zhang, Y. Genc, N. Navab, Taking AR into large scale industrial environments: Navigation and information access with mobile computers, IEEE and ACM International Symposium on Augmented Reality. (2001) 179-180.

[9] L. Naimark, E. Foxlin, Circular data matrix fiducial system and robust image processing for a wearable vision-inertial self-tracker, Proceedings of the 1st International Symposium on Mixed and Augmented Reality. (2002) 27-36.

[10] M. Rohs, Real-world interaction with camera phones, Ubiquitous Computing Systems. (2005) 74-89.

[11] X. Zhang, S. Fronz, N. Navab, Visual marker detection and decoding in AR systems: A comparative study, Proceedings of the 1st International Symposium on Mixed and Augmented Reality. (2002) 97-106.

[12] M. Fiala, ARTag, a fiducial marker system using digital techniques, Computer Vision and Pattern Recognition. (2005) 590-596.

[13] R. Hartley, A. Zisserman, Multiple view geometry in computer vision, Cambridge Univ. Press. (2000).

[14] Z. Zhang, A flexible new technique for camera calibration, IEEE Trans. Pattern Anal. Mach. Intell. 22 (11) (2000) 1330-1334.

[15] N. Otsu, A Threshold Selection Method from Gray-Level Histograms, IEEE Trans. Syst. Man. Cybern.9 (1) (1979) 62–66.

[16] R. Gonzales, R. Woods, Digital Image Processing, Pearson Education, (2009).

[17] D. Douglas, T. Peucker, Algorithms for the reduction of the number of points required to represent a digitized line or its caricature, Canadian Cartographer. 10 (2) (1973) 112-122.

[18] J. Matney, B. Parker, D. Neck, G. Henkelmann, I. Rosen, Target localization accuracy in a respiratory phantom using BrainLab ExacTrac and

4DCT imaging, J. Appl. Clin. Med. Phys. 12 (2) (2011).

저 자 소 개

우다야위제나야키(학생회원)
2010년 스리랑카 Colombo대학교 컴퓨팅학부 학사졸업.
2013년 경북대학교 대학원 컴퓨터학부 석사졸업.
2013년 경북대학교 대학원 컴퓨터학부 박사과정
<주관심분야 : 3D복원, 3D의료영상, 3D 모션추적>

박 순 용(평생회원)
1991년 경북대학교 전자공학과 학사졸업.
1993년 경북대학교 전자공학과 석사졸업.
2003년 미국 뉴욕주립대학교 스토니브룩 박사졸업.
1993년～1999년 한국원자력연구소 로봇기반연구실 선임연구원.
2004년～2005년 한국전자통신연구원 디지털콘텐츠연구단 선임연구원.
2005년～현재 경북대학교 컴퓨터학부 부교수.
<주관심분야: 3차원스캐닝, 3차원정합, 로봇비전, 3D프린팅>